IRAQI JOURNAL OF APPLIED PHYSICS
Vol. 22, No. 1, January-March 2026, pp. 12-18

Green Synthesis and Characterization of Bismuth Oxide Nanoparticles for Optoelectronic Applications

Edrees E. Khadeer [1]
Muhammad H. Shareef [1]
Mohanad H. Mohammed [2]

[1] Department of Physics, College of Science, University of Mosul, Mosul, 41200, IRAQ
[2] Nineveh Education Directorate, Ministry of Education, Mosul, 41200, IRAQ
* Corresponding author: noorhudahasan12567@gmail.com

The green synthesis of bismuth oxide nanoparticles (Bi_2O_3) using peppermint (Mentha pulegium) extract offers an eco-friendly, cost-effective, and scalable alternative to conventional methods. In this study, Bi_2O_3 nanoparticles were successfully synthesized and characterized using X-ray diffraction (XRD), scanning electron microscopy (SEM), and ultraviolet-visible (UV-Vis) spectroscopy. XRD analysis confirmed a polycrystalline tetragonal structure (β-phase) with an average crystallite size of 58.06 nm, while SEM revealed uniformly distributed nanogranular-like morphologies. Optical studies demonstrated strong UV absorption (320–400 nm) and high visible-light transmittance, with a direct bandgap of 2.4 eV. Notably, the extinction coefficient (K) exhibited a pronounced peak (~1500 a.u.) at 400–450 nm, while the refractive index (n) displayed normal dispersion behavior, decreasing sharply in the visible range before stabilizing in the near-IR region. These optoelectronic properties, classified the material as a semiconductor, highlight the nanoparticles' potential for UV shielding, solar cells, photocatalysis, and optoelectronic devices. The study underscores the efficacy of plant-mediated synthesis for producing functional nanomaterials with reproducible and tunable properties, aligning with sustainable development goals.

Keywords: Green synthesis; Bi_2O_3 nanoparticles; Peppermint extract; Optical properties
Received: 7 May 2025; Revised: 30 June 2025; Accepted: 7 July 2025; Published: 1 January 2026

1. Introduction

The biosynthesis of nanoparticles using plant extracts has revolutionized the production of metal and metal oxide nanoparticles by offering a sustainable alternative to conventional physical and chemical synthesis methods [1]. This approach utilizes biological agents such as plants, bacteria, fungi, and yeasts as natural reducers and stabilizers, significantly reducing environmental hazards and energy consumption [2]. The simplicity, cost-effectiveness, and eco-friendliness of this method align with global sustainability initiatives aimed at minimizing toxic waste and combating climate change [3]. Plant extracts - derived from leaves, flowers, fruits, seeds, bark, and other botanical parts - are rich in bioactive compounds, including flavonoids, phenolic acids, alkaloids, terpenoids, and proteins [1,4,5]. These biomolecules play a dual role in nanoparticle synthesis: they reduce metal ions to their nanoscale forms while simultaneously acting as capping agents to control particle size and morphology [3]. Among various nanomaterials, metal oxide nanoparticles have attracted significant interest due to their unique physicochemical properties, making them suitable for applications in catalysis, renewable energy, and environmental cleanup [6]. Bismuth oxide (Bi_2O_3) nanoparticles, in particular, exhibit exceptional properties such as low toxicity, high electrical conductivity, and an adjustable bandgap [7-18]. These features make them highly desirable for advanced technological and environmental applications, including [19-31]:

1. Solid-oxide fuel cells (SOFCs): Serving as efficient electrolytes for energy conversion.
2. Drug delivery systems: Exploiting their visible-light photocatalytic activity for targeted therapy.
3. Antibacterial applications: Effectively inhibiting pathogens like *E. coli* through photocatalytic mechanisms.
4. Water purification: Removing toxic heavy metals such as Chromium VI via adsorption and degradation.

Recent advancements have also highlighted Bi_2O_3 nanoparticles as excellent UV absorbers, with nanoscale particles outperforming bulk materials due to their enhanced surface-area-to-volume ratio [33–36]. While traditional synthesis techniques - such as sol-gel [24], hydrothermal [21], laser ablation [22], and chemical vapor deposition [29] - rely on hazardous chemicals and high energy inputs, green synthesis provides a cleaner and more sustainable alternative. By using plant extracts, this method avoids toxic reagents, lowers energy demands, and leverages renewable biological resources, making it both scalable and environmentally safe [30-32].

In this study, we introduce an efficient green synthesis method for Bi_2O_3 nanoparticles using *Mentha pulegium* (peppermint) extract, selected for its high concentration of bioactive compounds that promote effective nanoparticle reduction and stabilization. Through detailed characterization of the nanoparticles' structural and optical properties, we evaluate their

potential as UV-blocking agents and explore their applicability in high-value industries. This research contributes to the advancement of sustainable nanomaterial production while offering new insights into the development of functional materials for environmental and technological applications.

2. Experimental Methods

Fresh *Mentha pulegium* (peppermint) leaves were thoroughly cleaned using double-distilled water (DD water) to remove surface impurities. The washed leaves were air-dried in shaded conditions to prevent photochemical degradation of bioactive compounds, then pulverized into a fine powder using an electric grinder. For extract preparation, 10 g of the powdered leaves were refluxed in 100 mL of DD water at 90°C for 2 hours using a magnetic stirrer. The resulting mixture was cooled to room temperature, filtered through Whitman No.1 filter paper, and centrifuged at 4000 rpm for 30 minutes to obtain a clear supernatant. The nanoparticle synthesis was performed by dissolving 2 g of high-purity bismuth nitrate pentahydrate [$Bi(NO_3)_3$•$5H_2O$] (99.98%) in 10 mL of DD water at 90°C. This solution was then combined with 20 mL of the peppermint extract under continuous magnetic stirring (500 rpm) at 90°C for 18 hours, maintaining the volume of the solution throughout the heating period. The reaction was carried out under controlled temperature and stirring conditions to ensure uniform nanoparticle formation through biological reduction. The final product, as shown in Figure 1, demonstrated successful biosynthesis of bismuth oxide nanoparticles via this eco-friendly approach.

Fig. (1) The solution of Bi_2O_3 nanoparticles

Bismuth oxide (Bi_2O_3) thin films were deposited onto preheated glass substrates (300°C) via spray pyrolysis in an ambient atmosphere. The precursor solution was atomized and uniformly sprayed onto the substrates with precise flow rate control to ensure homogeneous film formation. A heat-resistant collector was placed beneath the spray nozzle to minimize droplet accumulation and prevent film defects. After deposition, the coated substrates underwent controlled cooling for 30 minutes to promote complete oxidation and crystalline growth while reducing thermal stress-induced cracking, yielding high-quality, adherent Bi_2O_3 thin films with optimal structural integrity. The crystalline structure of the synthesized Bi_2O_3 nanoparticles was analyzed using a Shimadzu XRD-6000 diffractometer with graphite-monochromatized CuKα radiation (λ = 1.54060 Å). The instrument was operated at 40 kV and 30 mA to assess phase purity and crystallographic properties. Morphological characterization was performed using a Nova NanoSEM 450 field-emission scanning electron microscope (FE-SEM), providing high-resolution surface imaging and microstructural analysis. The optical properties of the Bi_2O_3 thin films were examined using a Caihong 721-1000 UV-Vis spectrophotometer in single-beam mode. Baseline correction was applied by measuring the substrate blank before sample analysis. The absorption spectrum obtained allowed for determination of the bandgap energy and evaluation of the material's light-interaction properties, facilitating a comprehensive study of its photonic behavior.

3. Results and Discussion

The crystal structure of the bismuth oxide thin film was examined using X-ray diffraction (XRD) in the 2θ range of 5°–85°. As shown in Fig. (2), the XRD pattern exhibited sharp and distinct peaks corresponding to the (220), (240), (402), and (006) crystallographic planes, with the most intense peak observed at 2θ = 23.44° for the (220) orientation, suggesting a preferential growth direction. The well-resolved Bragg reflections confirmed the polycrystalline nature of the film. By comparing the diffraction data with the reference JCPDS card (96-900-7724) using Mach3 software, the film was identified to have a tetragonal crystal structure (β-Bi_2O_3), showing excellent agreement with the standard reference.

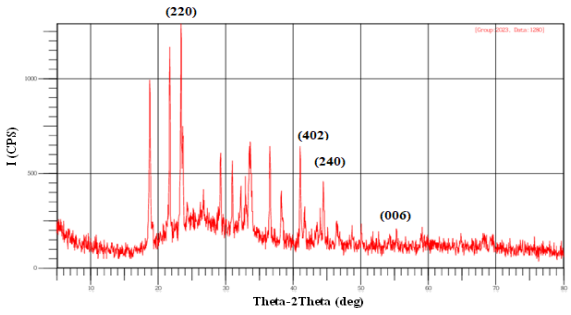

Fig. (2) XRD pattern of Bi_2O_3 nanoparticles

The average crystallite dimension of the synthesized bismuth oxide nanoparticles was calculated as 58.06 nm through application of the Debye-Scherrer equation ($D=K\lambda/\beta\cos\theta$) [37]. In this calculation, we employed a shape factor (K) of 0.91,

Cu-Kα radiation (λ = 1.54060 Å), and the full width at half maximum (β) of the (220) diffraction peak measured in radians. These XRD results demonstrate effective nanomaterial synthesis, with the calculated size confirming the development of structurally well-ordered nanocrystals.

Morphological examination via scanning electron microscopy at 5000x and 10000x magnifications revealed a homogeneous surface architecture consisting of tightly packed, uniformly dispersed nanograins covering the substrate surface (Fig. 3). The observed granular nanostructure shows excellent correlation with the tetragonal polycrystalline phase detected in XRD patterns, providing conclusive evidence for successful β-Bi_2O_3 nanoparticle formation. These experimental outcomes show remarkable consistency with the earlier findings reported by Motakef-Kazemi and Yaqoubi [2], particularly regarding the characteristic nanorod morphology, thereby substantiating the reliability of the fabrication process.

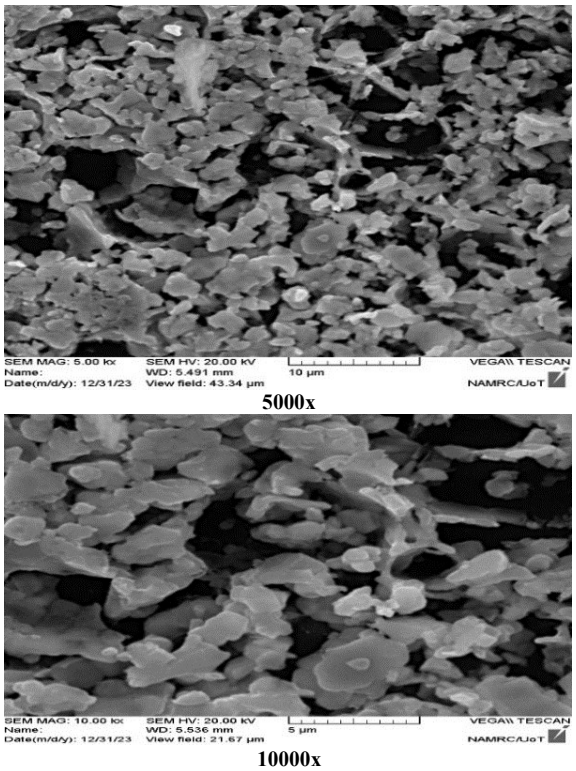

Fig. (3) SEM images of Bi_2O_3 nanoparticles

UV-Vis spectroscopic analysis (320-1000 nm) of the synthesized bismuth oxide thin film demonstrated characteristic absorption behavior (Fig. 4a). The spectrum exhibited a pronounced absorption onset in the UV region (320-400 nm) near the fundamental edge, with absorption tails persisting up to 550 nm in the visible range. This progressive decrease in absorption intensity with increasing wavelength reflects the material's bandgap limitations, where photon energies below the threshold become incapable of promoting electronic transitions. The absorption profile stabilized significantly beyond 770 nm in the NIR region, confirming the wide-bandgap semiconducting properties of the film. These optical characteristics suggest promising photovoltaic applications, particularly for devices requiring [38]:

1. Strong UV-visible photon harvesting (320-550 nm).
2. Infrared transparency for thermal management.
3. Tunable performance depending on implementation: As a transparent conductive oxide (TCO) in front electrodes, As an active absorber layer in heterojunction configurations

The observed spectral response correlates well with the requirements for next-generation solar cells that combine visible-light absorption with infrared transparency, while the exact performance would be application-specific based on the film's structural and electronic properties.

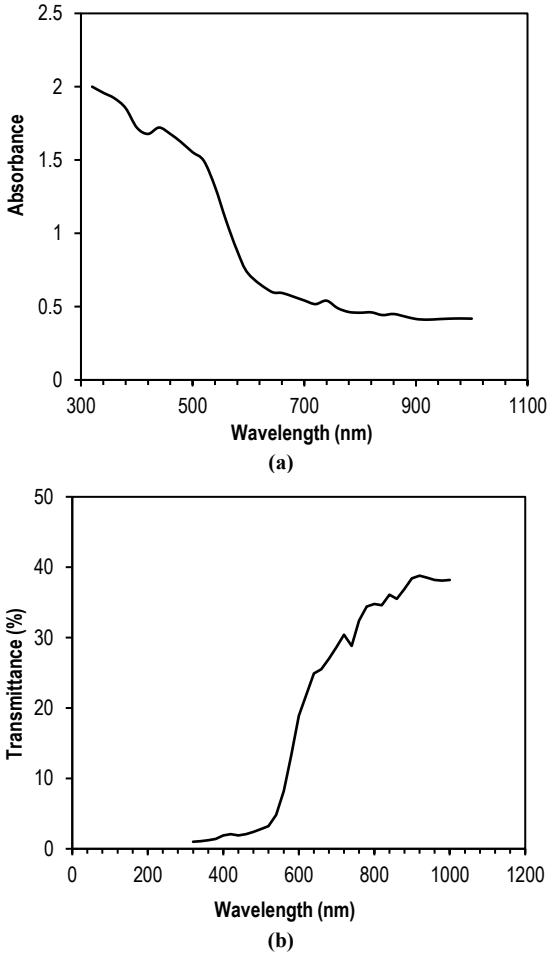

Fig. (4) Variation of absorbance (a) and transmittance (b) of Bi_2O_3 thin film as a function of wavelength

The transmittance spectrum of the bismuth oxide thin film, as shown in Fig. (4b), displayed an inverse correlation with its absorption profile, highlighting critical optoelectronic properties. Near the fundamental

absorption edge at shorter wavelengths, the film exhibited very low transmittance, with a clear cut-off wavelength indicating the shift from strong absorption to higher transmission. As the wavelength increased beyond this point, transmittance rose sharply before stabilizing in the near-infrared region (above 900 nm). This marked contrast in behavior - efficient visible light absorption coupled with high infrared transparency - underscores the film's strong potential for solar cell applications. Such a spectral response is ideal for photovoltaic systems, where effective visible photon harvesting and minimal energy loss from non-absorbable infrared radiation are essential. Additionally, these findings align with the material's wide bandgap semiconductor characteristics, supporting its viability for integration into advanced photovoltaic devices.

The reflectance (R) of the Bi_2O_3 thin film, calculated as the fraction of incident radiation energy reflected by the film, was derived using the energy conservation principle (R = 1 – A – T) [39], where A and T represent absorbance and transmittance, respectively. As illustrated in Fig. (5), the reflectance spectrum gradually decreased across the 320–1000 nm wavelength range, showing an inverse relationship with both absorption and transmission. At shorter wavelengths - where absorption was dominant - the film exhibited higher reflectance due to stronger photon interactions. Conversely, beyond the absorption edge, reflectance declined as transmittance increased. This systematic variation in reflectance highlights the film's wavelength-dependent optical behavior, making it a promising candidate for photonic applications that rely on selective light reflection.

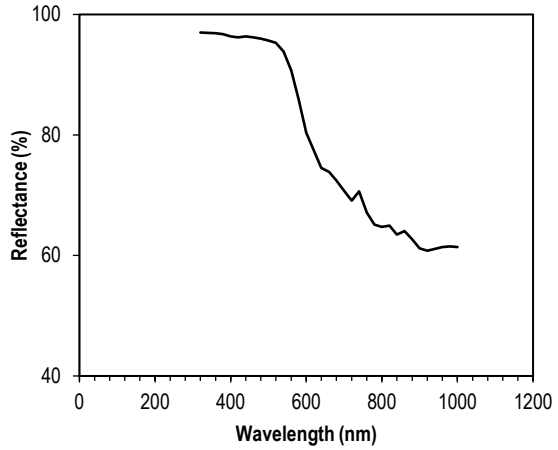

Fig. (5) Variation of reflectance of Bi_2O_3 thin film as a function of wavelength

The optical band gap of the synthesized bismuth oxide thin film was evaluated using Tauc analysis based on the Davis-Mott equation for direct transitions: $(\alpha h\nu)^2 = b(h\nu - E_g)$ [40], where α is the absorption coefficient ($\alpha=2.303A/t$ ($t=4.81541x10^{-5}m$)), hν is the photon energy, b is a material-dependent constant, and E_g represents the bandgap energy. As shown in Fig. (6), the bandgap was determined by extrapolating the linear portion of the $(\alpha h\nu)^2$ vs. hν plot to the x-axis intercept, corresponding to the point where $(\alpha h\nu)^2 = 0$. This analysis confirmed direct allowed transitions (n=2) and provided an accurate measurement of the semiconductor's optoelectronic properties, indicating its suitability for photonic applications. The well-defined linear region in the Tauc plot further underscores the high quality and structural integrity of the nanostructured film.

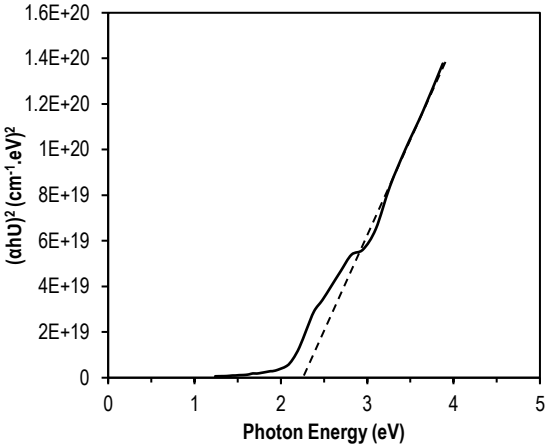

Fig. (6) Variation of $(\alpha h\nu)^2$ of Bi_2O_3 thin film as a function of photon energy ($h\nu$)

The nanostructured Bi_2O_3 thin film exhibits an optical bandgap of 2.4 eV, classifying it as a semiconductor with promising optoelectronic characteristics. This intermediate bandgap, derived from Tauc plot analysis, places the material between wide-bandgap insulators and narrow-bandgap semiconductors, making it well-suited for visible-light-driven applications. The 2.4 eV value corresponds to light absorption in the blue-green region (~515 nm), indicating potential utility in photodetectors, photocatalysis, and photovoltaic devices operating within this spectral range. The observed bandgap is consistent with the tetragonal crystal structure confirmed by XRD and the nanorod morphology revealed in SEM imaging, demonstrating structural-property coherence across characterization methods. The semiconductor behavior, coupled with the nanostructured morphology, enables tunable electronic properties, enhancing its applicability in advanced optoelectronics and solar energy conversion technologies. These findings align with recent research on green-synthesized Bi_2O_3 nanoparticles, such as the work by Motakef-Kazemi & Yaqoubi [2], who reported a similar direct bandgap of 2.4 eV and analogous UV-Vis absorption trends. Both studies highlight strong visible-light absorption (320–520 nm) and infrared transparency, reinforcing the material's potential for solar energy harvesting. While prior research emphasized UV shielding and antibacterial

applications, the consistent optical and structural properties across studies validate the reproducibility of plant-mediated Bi_2O_3 synthesis and its optoelectronic performance.

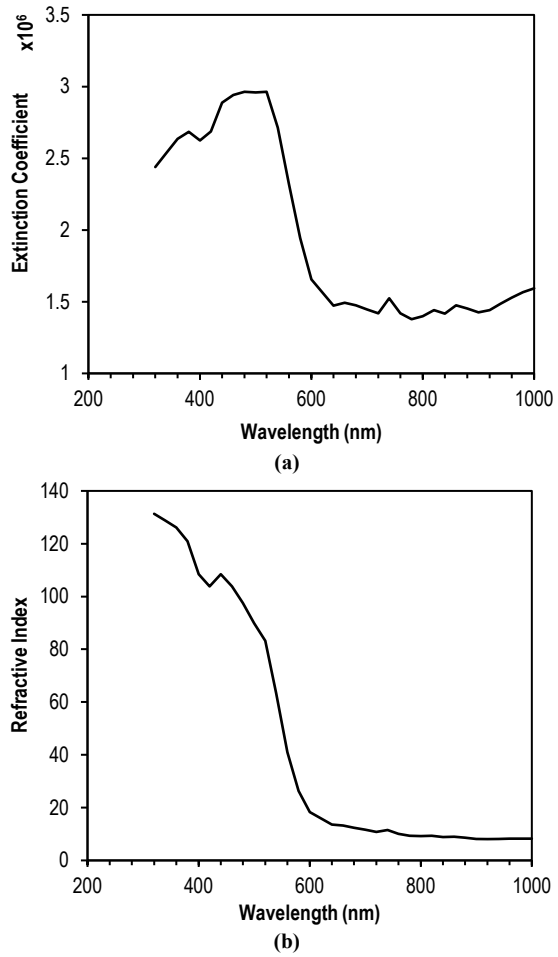

Fig. (7) Variation of extinction and refractive coefficients of Bi_2O_3 thin film as functions of wavelength

The optical properties of the Bi_2O_3 film provide key insights into its light-matter interactions. As shown in Fig. (7a), the extinction coefficient ($k=\alpha\lambda/4\pi$) [41] exhibits a distinct peak (~1500 a.u.) in the 400–450 nm wavelength range, indicating strong photon absorption due to band-to-band transitions near the absorption edge. Beyond this region, the extinction coefficient gradually decreases at longer wavelengths (520–1000 nm), confirming the material's semiconducting nature with dominant absorption in the visible (blue-violet) spectrum and increasing transparency in the infrared region. Complementary analysis of the refractive index ($n=(1+\sqrt{R})/(1-\sqrt{R})$) [41] reveals normal dispersion behavior (Fig. 7b), with a sharp decline in the visible range before stabilizing in the near-IR, a characteristic feature of wide-bandgap semiconductors. The strong correlation between the wavelength-dependent responses of k and n further validates the film's 2.4 eV bandgap and its high absorption efficiency in the visible range (400–600 nm) while remaining transparent to near-IR radiation. The consistency in these optical parameters underscores the high quality and uniformity of the nanostructured Bi_2O_3 film, reinforcing its potential for visible-light optoelectronic applications, including photodetectors, solar cells, and photocatalytic systems.

4. Conclusion

The green-synthesized Bi_2O_3 nanoparticles displayed a polycrystalline tetragonal structure, with an average crystallite size of 58.06 nm. Densely packed nanogranular morphologies with uniform substrate distribution was revealed. Strong UV absorption was indicated with peak absorbance occurring between 320 and 400 nm, alongside high reflectivity (~70% in the 320–500 nm range). The material exhibited a direct bandgap of 2.4 eV, along with notable visible-light absorption and infrared transparency. These properties - combined with its semiconductor characteristics and nanostructured morphology - make Bi_2O_3 nanoparticles promising for applications in UV shielding, solar cells, and optoelectronic devices, leveraging its semiconductor behavior and nanostructured morphology for enhanced performance.

Acknowledgment

The authors sincerely thank the University of Mosul, College of Science, for their financial support and access to essential research facilities, which were instrumental in achieving the objectives of this study.

References

[1] H.H. Azeez, H.H. Hasan and H.H. Karim, "Green Synthesis ZnO NPs and Their Effects on Plant Growing", *Coll. Basic Edu. Res. J.*, 20(2.1) (2024) 103.

[2] N. Motakef-Kazemi and M. Yaqoubi, "Green synthesis and characterization of bismuth oxide nanoparticle using Mentha pulegium extract", *Iranian J. Pharmaceut. Res.,* 19 (2020) 70-79.

[3] U. Shanker, C.M. Hussain and M. Rani, **"Green nanomaterials for industrial applications"**, Elsevier (2022).

[4] S.A. Aromal and D. Philip, "Green synthesis of gold nanoparticles using Trigonella foenum-graecum and its size-dependent catalytic activity", *Spectrochim. Acta A*, 97 (2012) 1–5.

[5] F. Tavakoli, M. Salavati-Niasari and F. Mohandes, "Green synthesis and characterization of graphene nanosheets", *Mater. Res. Bull.*, 63 (2015) 51-57.

[6] P. Falcaro et al., "Application of metal and metal oxide nanoparticles@MOFs", *Coord. Chem. Rev.*, 307 (2016) 237–254.

[7] V. Mane et al., "A review on Bi_2O_3 nanomaterial for photocatalytic and antibacterial applications", *Chem. Phys. Impact*, 8 (2024) 100517.

[8] H.T. Fan et al., "δ-Bi_2O_3 thin films prepared by reactive sputtering: Fabrication and characterization", *Thin Solid Films*, 513 (20066) 142–147.
[9] W. Raza et al., "Synthesis, characterization and photocatalytic performance of visible light-induced bismuth oxide nanoparticle", *J. Alloys Compd.*, 648 (2015) 641–650.
[10] Y. Gong et al., "Performance of (La,Sr)MnO_3 cathode-based solid oxide fuel cells: Effect of bismuth oxide sintering aid in silver paste cathode current collector", *J. Power Sources*, 196 (2011) 928–934.
[11] X. Gou et al., "Room-temperature solution synthesis of Bi_2O_3 nanowires for gas sensing application", *Nanotech.,* 20 (2009) 495–501.
[12] P. Malik and D. Chakraborty, "Bi_2O_3-catalyzed oxidation of aldehydes with t-BuOOH", *Tetrahedron Lett.*, 51 (2010) 3521–3523.
[13] F. Xia et al., "Preparation of bismuth nanoparticles in aqueous solution and catalytic performance for the reduction of 4-nitrophenol", *Ind. Eng. Chem. Res.*, 53 (2014) 10576–10582.
[14] M. Schlesinger et al., "Metastable β-Bi_2O_3 nanoparticles with potential for photocatalytic water purification using visible light irradiation", *Chemistry*, 2 (2013) 146–155.
[15] W.E. Mahmoud and A.A. Al-Ghamdi, "Synthesis and properties of bismuth oxide nanoshell-coated polyaniline nanoparticles for promising photovoltaic properties", *Polym. Adv. Technol.*, 22 (2011) 877–881.
[16] M.J. Oviedo et al., "New bismuth germanate oxide nanoparticle material for biolabel applications in medicine", *J. Nanomater.*, 2016 (2016) https://doi.org/10.1155/2016/9782625.
[17] A.M.N. Jassim et al., "Study the antibacterial effect of bismuth oxide and tellurium nanoparticles", *Int. J. Chem. Biol. Sci.*, 1 (2015) 81–84.
[18] N. Nurmalasari, Y. Yulizar and D.O.B. Apriandanu, "Bi_2O_3 nanoparticles: Synthesis, characterizations, and photocatalytic activity", Department of Chemistry, Faculty of Mathematics and Natural Sciences (FMIPA), Universitas Indonesia, Depok 16424, Indonesia. doi: 10.1088/1757-899X/763/1/012036.
[19] J. La et al., "Synthesis of bismuth oxide nanoparticles by solution combustion method", *Particul. Sci. Technol.*, 31 (2012) 287–290.
[20] J. Wu et al., "Solvothermal synthesis of uniform bismuth nanospheres using poly(N-vinyl-2-pyrrolidone) as a reducing agent", *Nanoscale Res. Lett.*, 6 (2011) 66–74.
[21] Z.A. Zulkifli et al., "Synthesis and characterisation of bismuth oxide nanoparticles using hydrothermal method: The effect of reactant concentrations and application in radiotherapy", *J. Phys. Conf. Ser.*, (2018) doi: 10.1088/1742-6596/1082/1/012103.
[22] M.H. Mohammed, M.N. Hussein and A.K.A. Suleiman, "Effect of Deposition Method on Optical and Structural Properties of Bismuth Oxide Thin Films", *Iraqi J. Appl. Phys.*, 21(1) (2025) 71-74.
[23] S. Anandan and J.J. Wu, "Microwave-assisted rapid synthesis of Bi_2O_3 short nanorods", *Mater. Lett.*, 63 (2009) 2387–2389.
[24] M. Mallahi et al., "Synthesis and characterization of bismuth oxide nanoparticles via sol-gel method", *Adv. J. Eng. Res.*, 3 (2014) 162–165.
[25] L. Mädler and S.E. Pratsinis, "Bismuth oxide nanoparticles by flame spray pyrolysis", *J. Am. Ceram. Soc.*, 85 (2004) 1713–1718.
[26] G. Carotenuto et al., "Synthesis and thermoelectric characterisation of bismuth nanoparticles", *J. Nanopart. Res.*, 11 (2009) 1729–1738.
[27] T.P. Gujar et al., "Formation of highly textured (111) Bi_2O_3 films by anodization of electrodeposited bismuth films", *Appl. Surf. Sci.*, 252 (2006) 2747–2751.
[28] T.P. Gujar, V.R. Shinde and C.D. Lokhande, "The influence of oxidation temperature on structural, optical and electrical properties of thermally oxidized bismuth oxide films", *Appl. Surf. Sci.*, 254 (2008) 4186–4190.
[29] R.Z.A. Al-Fulayih et al., "Preparation of CdTe thin films using seed method", *Func. Mater.*, 31(3) (2024) 377-380.
[30] P. Nazari et al., "Biosynthesis of bismuth nanoparticles using *Serratia marcescens* isolated from the Caspian Sea and their characterization", *IET Nanobiotechnol.*, 6 (2012) 58–62.
[31] S. Mondal et al., "Biogenic synthesis of Ag, Au and bimetallic Au/Ag alloy nanoparticles using aqueous extract of mahogany (Swietenia mahogani JACQ.) leaves", *Colloid Surf. B*, 82 (2011) 497–504.
[32] R. Dobrucka, "Synthesis of titanium dioxide nanoparticles using *Echinacea purpurea Herba*", *Iran. J. Pharma. Res.*, 16 (2017) 753–759.
[33] R. Senthamilselvi and R. Velavan, "Microstructure and photocatalytic properties of bismuth oxide (Bi_2O_3) nanocrystallites", *Malaya J. Matematik*, 2 (2020) 4870–4874.
[34] N. Motakef-Kazemi and M. Yaqoubi, "Green synthesis and characterization of bismuth oxide nanoparticle using *Mentha pulegium* extract", *Iranian J. Pharma. Res.,* 19 (2020) 70-79.
[35] A. Becheri et al., "Synthesis and characterization of zinc oxide nanoparticles: Application to textiles as UV-absorbers", *J. Nanoparticle Res.*, 10 (2008) 679–689.
[36] Y.M. Im et al., "Effect of ZnO nanoparticles morphology on UV blocking of poly(vinyl

alcohol)/ZnO composite nanofibers", *Mater. Lett.*, 147 (2015) 20–24.
[37] A.A. Sulaiman, "Effect of γ-Irradiation on the n-Porous Silicon Structures Prepared by Electrochemical Etching", *Rafidain J. Sci.*, 27(3) (2018) 173-180.
[38] K. Yoshikawa et al., "Silicon heterojunction solar cell with interdigitated back contacts for a photoconversion efficiency over 26%", *Nat. Energy*, 2 (2017) 17032.
[39] M. Al-Azow et al., "Preparation of Silver Nanoparticles By Nd:YAG Pulsed Laser and Study Their Optical and Structural Properties", *J. Edu. Sci.*, 34(2) (2025) 13-23.
[40] E.E. Ghadeer, R.Z.A. Al-Fulayih and Z.B. Ibraheem, "Study of the effect of adding glass and carbon powders on optical behavior of unsaturated polyester resin", *AIP Conf. Proc.*, 2394 (2022) 090023.
[41] E.E. Khadeer, M.A. Abed and M.A. Hmood, "The Optical Properties of Unsaturated Polyester Reinforcement by Glass Fibers", *Jordan J. Phys.*, 17(2) (2024) 155-163.

